EFDA–JET–PR(10)64

S.J.P. Pamela, G.T.A. Huysmans, M.N.A. Beurskens, S. Devaux, T. Eich,
S. Benkadda and JET EFDA contributors

Nonlinear MHD Simulations of ELMs in JET

Nonlinear MHD Simulations of ELMs in JET

S.J.P. Pamela[1], G.T.A. Huysmans[1],
M.N.A. Beurskens[2], S. Devaux[3], T. Eich[3], S. Benkadda[4]
and JET EFDA contributors*

JET-EFDA, Culham Science Centre, OX14 3DB, Abingdon, UK

[1]Association EURATOM-CEA, F-13108 Saint-Paul-lez-Durance, France
[2]JET-EFDA, Culham Science Centre, OX14 3DB, Abingdon, OXON, UK
[3]Max-Planck Institut fur Plasmaphysik, EURATOM-Assoziation, D-85748, Garching, Germany
[4]PIIM, CNRS - University of Provence, St. Jérôme, Case321, 13397 Marseille Cedex20, France
** See annex of F. Romanelli et al, "Overview of JET Results",*
(23rd IAEA Fusion Energy Conference, Daejon, Republic of Korea (2010)).

Preprint of Paper to be submitted for publication in
Plasma Physics and Controlled Fusion

ABSTRACT

Nonlinear MHD simulations with the JOREK code may be used to improve our understanding of Edge-Localised-Modes (ELMs) [1,2,3]. These H-mode related instabilities may cause some damage to the tungsten divertor of ITER [4], and it was demonstrated experimentally that the ELM energy losses increase with both machine size and decreasing collisionality [5,6]. In sight of producing simulations of ELMs in ITER, in order to give some predictions of ELM size and divertor heat-fluxes in the future device, simulations first need to be quantitatively validated against experimental data of present machines.

This paper presents simulations of ELMs in the JET tokamak, for the low-collosionality type-I ELMy Hmode Pulse No: 73569. The simulation results are compared to experimental data to provide a qualitative validation of simulations. This comparison comprises the dynamics of filaments and divertor heat-fluxes, the effect of resistivity and collisionality on ELM energy losses, and the observation of ELM precursors prior to the pedestal collapse.

1. INTRODUCTION

1.1 GOALS AND MOTIVATION

At present, it is commonly agreed that the most successful tokamak scenario, in view of producing fusion energy, is the type-I ELMy H-mode. In fact, Edge-Localised-Modes are necessary for steady plasma operation, since they evacuate the excess of density and impurities from the plasma core. The type-I ELMy H-mode is planned to be the basis operational scenario for the future device ITER. However, and although ELMs are necessary, these instabilities may cause some rapid erosion of some Plasma-Facing Components - especially the tungsten divertor [4]. In fact, it is natural that the amount of energy released by ELMs increases proportionally with the machine size, leading to larger ELM heat-fluxes in larger machines such as ITER and DEMO. But in addition to the increase in size, it has been shown in some experimental studies that when going towards lower collisionality - higher temperatures needed for fusion - the amount of ELM energy losses relative to the pedestal energy $\Delta W_{ELM}/W_{ped}$ increases as well [6]. Together, these two predictions prospect that large type-I ELMs in ITER will cause heat-fluxes that could significantly damage divertor materials, which would in turn limit plasma operation. There are some ELM-control tools and techniques - Resonant Magnetic Perturbations, pellets, kicks - which were developed to reduce the impact of ELMs on the PFCs, but although these tools work reasonably well, the understanding of their mechanism is yet poor. The understanding of basic ELM physics could help determine the mechanisms of ELM-control tools, and it could also help predict the size of ELMs and related heat-fluxes in bigger devices. In addition, advanced knowledge of ELM physics could be used to develop new ELM-control tools.

There is already some advanced knowledge of linear MHD properties of ELMs, relying on the peelingballooning theory for stability limits of edge currents and pedestal pressure gradients [7,8,9,10]. There are also some intuitions that ELMs would be caused by the pedestal pressure gradient rather than the parallel current at the edge [11,12]. And some work has also been dedicated

to the nonlinear behaviour of ELMs, with mainly two different opinions: that ELMs are explosive instabilities [13], or that ELMs are interchange-like instabilities [14]. However, a most efficient way to improve our understanding of the nonlinear evolution of ELMs remains the numerical simulations. Many nonlinear codes have been developed in recent years [1,15,16,17], and their results are all in reasonable qualitative agreement, both with one another, but also with experimental observations. In particular, a filamentation of the plasma edge into the Scrape-Off Layer (SOL) is observed, with strong heat-fluxes on the divertor and a significant ergodization of the separatrix. In this paper, simulations of the 3D nonlinear MHD code JOREK are presented.

Although nonlinear simulations of ballooning modes may be used to improve our understanding of some basic ELM physics, relying on qualitative comparisons with experiments (filaments, heat-fluxes), a more advanced understanding should rely on a robust, quantitative validation of simulations against experimental data. In particular, nonlinear simulations may be used to give coherent predictions for ITER only if the numerical code has first been thoroughly validated. In sight of providing such a quantitative validation against experiments, one first needs to produce simulations of realistic plasmas, with correct magnetic geometry, and pressure and current profiles. Here, we present simulations of Edge-Localised-Modes for the JET tokamak, using the type-I ELMy H-mode Pulse No: 73569, referenced as a low collisionality shot [18]. The study is laid out as follows. The second part of this section introduces the basic characteristics of the JOREK code, including the reduced MHD equations used for simulations. Section2 describes how experimental data for Pulse No: 73569 has been used to provide a coherent plasma equilibrium in JOREK, respecting the magnetic geometry of JET, and using pre-ELM pressure profiles with steep pedestal gradients. In the second part of Section2, this JET equilibrium is tested for its ideal MHD stability with respect to ballooning modes, using the HELENA equilibrium code [19], and the effect of the equilibrium poloidal rotation on the linear stability of ballooning modes is studied, as in [3]. Section3 deals with the simulation of ELMs using this JET equilibrium as a basis; it is divided into three sub-sections. The first part concerns the filamentation of the plasma edge into the SOL, the second part describes divertor heatfluxes and parallel transport in the SOL, and the third part aims at a qualitative validation of simulations by producing collisionality scans for the ELM size. Section4 ends the paper with an overview of the results and future prospects. These simulation results are compared to experimental observations.

1.2 THE NUMERICAL TOOL: JOREK

The JOREK code is a 3D nonlinear MHD code that has been developed with the specific aim to produce simulations of Edge-Localised-Modes [1,20]. It uses a poloidal grid built with isoparametric cubic Bezier finite elements [20], which are a generalization of the Hermite finite elements used in the HELENA equilibrium code [19]. The advantage of this generalization is that Bezier elements enable the refinement of isolated grid elements, although such localised refinement is not used for the simulations presented in this paper. The isoparametric property of the elements means that the

continuity of all variables and their derivatives is satisfied, including the poloidal space coordinates (R,Z). This finite element grid is aligned to equilibrium flux surfaces for both closed and open flux surfaces in X-point geometry, thus representing the three regions of the core, the Scrape-Off-Layer and the private region. The alignment of the grid with open flux surfaces in the SOL enables accurate treatment of fast parallel transport of energy along magnetic field lines. The toroidal dimension is represented by Fourier series.

The time-discretization is done using the fully implicit Crank-Nicholson scheme for all equations, so that temporal evolution is not restricted by the grid size, as in explicit schemes. The size of time steps depends mainly on the nonlinearity of the simulation. This implicit scheme results in a sparse system of equations, which are solved using a Generalized Minimal REsidual Solver (GMRES). The preconditioner for this iterative GMRES is obtained by solving independently each sub-matrix corresponding to different harmonics, which amounts to a block-Jacobi preconditioner. These sub-matrices are solved using the direct parallel sparse matrix solver PaStiX [21].

The simulations presented below were run with two different poloidal grids: a standard resolution grid and a high resolution grid. The standard grid is composed of 50 radial elements, 200 poloidal elements and additional SOL elements, which amounts to a total of ~15,000 elements. This grid was used to obtain the general results of ELMs simulations presented in Sections 3.1 and 3.2. The higher resolution grid is composed with 70 radial elements (~22,000 elements in total) and in addition the radial distribution of elements has a higher concentration near the separatrix. The aim of this grid was to obtain simulations of plasmas with steep pressure gradients in the pedestal region, and with low resistivity, reaching near-Spitzer values. Most simulations presented below were run for one toroidal mode number, on parallel computers, varying between 128 and 512 CPUs for the highest resolution grids. The simulations with high resolution grids were run on the HPC-FF (Juelich, Germany).

The MHD model solved for the simulations presented below is similar to that used in [3]. It is a two-fluid, reduced MHD model for the six variables (poloidal magnetic flux), (electric potential), $v_{||}$ (parallel velocity), ρ (density), T_i (ion temperature) and T_e (electron temperature). The reduction of the equations used here is based on the ansatz that the perpendicular velocity lies in the poloidal plane, and that the toroidal magnetic field is constant in time, so that the total plasma velocity and the total magnetic field are expressed respectively as

$$v = v_{||} + v_{\perp} = v_{||} B + R e_{\phi} \times \nabla \Phi \tag{1}$$

$$B = B_{\phi} + B_p = \frac{F_o}{R} e_{\phi} + \frac{1}{R} \nabla \psi \times e_{\phi} \tag{2}$$

where R is the major radius in toroidal geometry, e_ϕ is the toroidal unit vector and $F_o = B_o R_o$, with the magnetic field strength B_o at the magnetic axis $R = R_o$. Substituting these two ansatz into the visco-resistive MHD equations leads to the so-called reduced model, first derived by H.R. Strauss

[22], with two distinct equations for the parallel and perpendicular momentum,

$$R\nabla\cdot\left[R^2\rho\nabla_\perp\left(\frac{\partial\Phi}{\partial t}\right)\right] = [R^4\rho W,\,\Phi] - \frac{1}{2}\,[R^2\rho,\,R^4,|\nabla_\perp\Phi|^2] - [R^2,\,p] + [\psi,\,j] - \frac{F_o}{R}\,\frac{\partial j}{\partial\phi} + \mu R\nabla^2 W, \tag{3}$$

$$\rho F_0^2\,\frac{dv_\parallel}{dt} = F_0\,\frac{\partial p}{\partial\phi} - R\,[\psi,\,p] + \mu_\parallel\,\nabla^2 v_\parallel \tag{4}$$

$$\frac{\partial\rho}{\partial t} = \eta\,(j - j_A) + R\,[\eta,\,\Phi] - \frac{\partial\Phi}{\partial\phi} \tag{5}$$

$$\frac{\partial\rho}{\partial t} = -\nabla\cdot(\rho v) + \nabla\,(D_\perp\,\nabla_\perp\rho) + S_\rho \tag{6}$$

$$\rho\,\frac{\partial T_j}{\partial t} = -\rho v\cdot\nabla T_j - (\gamma-1)p\nabla\cdot v + \nabla\cdot(k_{\parallel j}\,\nabla_\perp T_j + k_{\parallel j}\,\nabla_\parallel T_j) + S_{T_j} \tag{7}$$

where the parallel current j, the toroidal vorticity W and the plasma pressure p are defined by

$$j = -R^2\nabla\phi\cdot J = \frac{1}{\mu_0}\,\Delta^*\psi \tag{8}$$

$$W = \nabla\phi\cdot(\nabla\times v_\perp) = \nabla_\perp^2\Phi \tag{9}$$

$$p = \rho\,(T_i + T_e) \tag{10}$$

where $\Delta^*\psi = R^2\nabla\left(\frac{\nabla\psi}{R^2}\right)$ is the Grad-Shafranov operator. The Poisson brackets used in the equations above are defined by $[a, b] = e_\psi\cdot(\nabla a\times\nabla b)$, and the convective derivative is defined by $d/dt = \partial/\partial t + v\cdot\nabla$. Also, the parallel gradient operator is defined by $\nabla_\parallel = (\mathbf{B}/B2)\mathbf{B}\cdot\nabla$. The density and temperature sources S_ρ and S_{Tj} have been introduced in the equations, and the perpendicular mass and thermal diffusivities $D_\perp$ and $\kappa_{\perp j}$ used in simulations are ad-hoc coefficients with a well at the pedestal region to represent the H-mode transport barrier. A Spitzer-like resistivity $\eta = \eta_o(T_e/T_{e,o})^{-3/2}$ is used, with $T_{e,o}$ the electron temperature at the magnetic axis. The Braginskii parallel thermal conductivities $\kappa_{\parallel j}$ are expressed as

$$k_{\parallel i} = k_{\parallel o}\,T_j^{5/2} \tag{11}$$

where the ratio of electron to ion parallel conductivity has been set to $k_{\parallel o,e}/k_{\parallel o,i} = 40$, which results from the smaller electron mass [23]. It should be noted that this set of equations is equivalent to that derived in [24], where energy of the system is shown to be conserved at first order.

The normalization used for these equations is based on the two quantities μo (magnetic permeability) and ρ_o (core density), so that time is normalized to a near Alfven time $\tilde{t} = t/\sqrt{\mu_o\rho_o}$. For a deuterium plasma with particle density $n_o = 6.10_{19}m^{-3}$, a normalized time unit corresponds

to 0.7μs. Naturally, current is normalized with μo and density with ρ_o. Pressure is also normalized with μo, and the diffusive parameters are normalized as $\tilde{\eta} = \eta \sqrt{\rho_o/\mu_o}$, $\tilde{\mu} = \mu \sqrt{\mu_o/\rho_o}$, $\tilde{D}_\perp = D_\perp \sqrt{\mu_o \rho_o}$ and $\tilde{\kappa}_\perp = \kappa_\perp \mu_o/\rho_o$,. Note that the parallel thermal conductivity depends explicitly on temperature, so that $k_{\|o}$ varies as $k_{\|o} \sim \rho_o^{-3}$. This will be important in Section3.2, where a scan in collisionality is obtained by varying ρ_o. The plasma boundary in the SOL is taken to be a flux surface, usually around 10cm away from the separatrix. On this boundary, Dirichlet conditions are applied for all variables (ie. perturbations of the equilibrium quantities are set to zero) except for temperature and density, which have Neumann conditions with null gradient. At the divertor targets, Mach-1 (Bohm) conditions are used for the parallel velocity, and the temperature and density have free outflow boundary conditions. In the private region, which is bounded by a flux surface, Dirichlet conditions are used for all variables.

2. RECONSTRUCTING THE JET EQUILIBRIUM

2.1 FROM EXPERIMENTS TO SIMULATIONS

The JET Pulse No: 73569 has been chosen for simulations. It is a standard type-I ELMy H-mode with constant NBI power, resulting in a regular ELM frequency and regular ELM size. This plasma pulse has a low triangularity (0.17), a total injected NBI power of 12.5MW, a magnetic field of 2T and a plasma current of 2.2MA. The pedestal electron density and temperature are respectively $5.10^{19} m^{-3}$ and 0.9keV, giving toroidal and poloidal betas of 2.2% and 0.66 respectively. The edge safety factor is $q_{95} \approx 3$. The collisionality is relatively low ($0.1 < \nu^* < 0.2$), and this shot was used for pedestal studies with High- Resolution Thomson Scattering (HRTS) [18]. The ELM frequency is 20Hz, and the ELM size is on average 0.25MJ, which is about 10% of the pedestal energy.

The two criteria for choosing this specific pulse was that it combines a good Infra-Red camera diagnostic [26,25] together with good HRTS profiles. The magnetic configuration used for this shot results in the outer strike point arriving on tile 5 of the outer divertor, so that the orientation of the IR-camera produces full views of the outer divertor heat fluxes during ELM crashes, which provides a comparison basis for simulations. Both temporal and spacial resolutions of the JET IR-camera are high enough to deal with ELMs dynamics (1 frame every 35μs with a 1.7mm resolution). Good HRTS profiles, together with a regular ELM frequency and ELM size, were required for the reconstruction of the plasma equilibrium in simulations. The pre-ELM HRTS electron density and temperature profiles are selected to obtain a pressure profile, which is used as input to solve the Grad-Shafranov equilibrium. Here, pre-ELM profiles means these are taken between 70 and 95% of the ELM period, when the pressure gradients are steepest. The combination of all pre-ELM profiles provides a good spacial resolution in the pedestal, in particular because horizontal shifts of the plasma are performed during the shot. These slight sweeps do not affect the plasma equilibrium, but enable a scanning of the whole pedestal region with the HRTS [18]. The pre-ELM HRTS profiles for the pulse are shown in Fig.1a, together with the fits used for simulations. Note that $T_i = T_i$ has been assumed for the initial equilibrium profiles in simulations.

In addition to the pressure profile obtained from the HRTS diagnostic, the reconstruction of theplasma equilibrium also requires a current profile and a flux boundary around the plasma, in order to solvethe Grad-Shafranov equation. Both these ingredients are taken from the EFIT equilibrium reconstruction. The global plasma current is that of EFIT, but an additional bootstrap current is also included to obtain the final profile. This bootstrap current is calculated with the HELENA equilibrium code using the Sauter model [27], for the corresponding pressure profile obtained from the HRTS. The flux contour is taken just around the first vessel wall, so that the resulting plasma equilibrium has a SOL size that corresponds approximately to that of JET. The final reconstruction is shown in Fig.1b, where it can be compared to the EFIT equilibrium.

2.2 LINEAR STABILITY OF THE EQUILIBRIUM

This equilibrium has been tested for its linear stability with respect to ballooning modes. The calculations were done with the equilibrium code HELENA for the ballooning mode number $n = \infty$, with ideal MHD equations. The resulting shows that the JET equilibrium, with the HRTS pressure profile, is ideally unstable. A scan in pressure gradient was performed by varying the pedestal pressure gradient width, and each case was tested with HELENA. The result, shown in Fig.2a, indicates that the JET equilibrium is indeed well above the ideal MHD stability limit.

However, the MHD model solved in the simulations is not ideal, and all diffusive parameters play a crucial role regarding the linear stability of the equilibrium. The resistivity has an enhancing effect on ballooning modes, so that linear growth rates of modes increase with increasing . All other diffusive parameters (μ, $D_\perp$ and $\kappa_\perp$) have the opposite effect: they damp ballooning modes growth rates. This is illustrated in Fig.2b, which shows a scan for the growth rate of the ballooning mode $n = 12$, as a function of resistivity and viscosity. All these diffusive parameters are strongly limited by numerical limits, since the lower diffusivity, the smaller eddies. Actual grid resolutions do not enable simulations with all diffusive parameters at correct values (experimental or at least theoretical values). Hence, one should bear in mind that no matter how ideally unstable a plasma equilibrium is, the resulting non-ideal ballooning mode simulations may result in stable modes (and vice-versa). For example, if resistivity is taken to be very low, but other parameters are taken relatively high (so that the mode is damped), the growth rates of ballooning modes might remain close to zero. The importance of this issue will be addressed again in Section3.3.

The other aspect of the equilibrium that may affect the linear stability of ballooning modes, and which is not taken into account in the HELENA calculations, concerns the poloidal equilibrium flow. A thorough study of such $\mathbf{E} \times \mathbf{B}$ flows at equilibrium, and their effect on ballooning modes, can be found in [3]. The circular ($m = 0$), pedestal rotation of the plasma for the JET equilibrium is observed to be particularly strong and sheared, and the consequent effect on the linear stability of ballooning modes is well identified. Fig.3a shows the poloidal flow structure for the JET equilibrium, which is the typical structure observed in simulations of realistic tokamak plasmas. Fig.3b shows the corresponding mid-plane profile for the poloidal rotation together with the density, to illustrate

that the flow is localised at the pedestal pressure gradient. The effect of the flow on the linear stability of ballooning modes is shown in Fig.3c, where growth rates are calculated for a range of ballooning mode numbers, with and without equilibrium flow. Without equilibrium flow means that the flow is artificial forced to zero. The damping effect of the flow is strongest for high mode numbers. It should also be noted that the poloidal flow may have a significant influence on the nonlinear behaviour of ballooning modes. In particular, the poloidal flow may stabilize ballooning modes and lead to ELM-like multiple bursts [3].

3. SIMULATIONS OF ELMS

3.1 GENERAL RESULTS: FILAMENTS

In ELMs simulations, there are two characteristics that stand out and that deserve some particular attention. The first one is the filamentation of the pedestal plasma into the Scrape-Off Layer, and the second one is the heat flux arriving on the divertor targets via parallel transport of energy along open magnetic field lines in the SOL. These two properties of ELMs, which are observed both in experiments and simulations, can be considered separately, but it may also be shown that they are strongly linked by the perturbation of the ballooning mode. In fact, the kinetic and magnetic components of the ballooning mode are but one perturbation, and the dynamics of filaments can be correlated to the dynamics of divertor heat-fluxes.

Before considering the link between these two phenomena, one first needs to consider the filaments themselves. It should be pointed out that in most ELMs simulations, multiple sets of filaments are repetitively ejected from the plasma, and those filaments have both poloidal and radial motion. Different sets of filaments may also entangle and get mixed with one another. Sometimes, filaments may even cross the separatrix and get sucked back into the plasma at a later time. Thus, the dynamics of filaments is rather complex, and to avoid confusion, the following study is performed only for the first set of filaments that leaves the pedestal. This brings some confidence as to the stability of the plasma at that moment, because the pedestal pressure is known (unperturbed), and the growth rate of the ballooning mode can be well identified, given the long linear exponential growth of the mode preceding the formation of the filaments.

The first characterization of filaments concerns their composition. The ballooning mode perturbs all MHD variables, but it is convenient to rely on one of these at first and then refer to it when considering other compositions of the filaments. The density is chosen to be this basis for comparison. The temperature inside a density filament is generally found to be rather significant, so that filaments can be said to be warm. A natural comparison with experiments consists in taking radial profiles of filaments, as with the HRTS diagnostic. In simulations, it is straight forward to obtain such profiles, but it is not so trivial to observe filaments with the HRTS, and given the tedious effort needed to obtain such profiles, comparisons are not made with the HRTS profiles from Pulse No: 73569, but with profiles presented by Beurskens et al. in [18], for Pulse No: 70553. As seen from Fig.4a, both the composition of the filament and its size are qualitatively well reproduced

by simulations. In particular, there is a large amount of density carried in the filament, with a hole (or well) of density forming behind the filament, which shows that the filament clearly separates from the main plasma. There is also a significant amount of electron temperature in the filament, which agrees with experiments. In fact, it is possible in simulations to compare electron and ion temperatures in the filaments: due to higher parallel conductivity for T_e, the electron temperature is evacuated from the filament more rapidly than T_i, which is illustrated in Fig.4b, with a 2D (poloidal) plot of a filament crossing the separatrix for ρ, T_i and T_e.

In addition to density and temperatures, there may also be some current crossing the separatrix. In previous simulations of standard plasmas, some current was also observed to be carried in the filaments. However, simulations of JET have a particularity that was not observed for other plasmas: the current is localised at the front gradient of the density filament, whereas all other previous simulations, including JET-like simulations, have filaments where density and current are almost perfectly in phase. To illustrate this, Fig.5a shows a HRTS-like radial profile of a filament for both density and current. In some extreme cases, where the growth rate of the ballooning mode is low, the density filament does not cross the separatrix because it is sheared by a poloidal flow. In such cases, only current crosses the separatrix. This
is illustrated in Fig.5b, which shows the time evolution of a density filament, together with current.

This latter point raises another characteristic of filaments: their speed. Filaments have both poloidal and radial motion, but although their poloidal speed can be well identified, it is not clear whether there is much variation in their radial speed. For example, Fig.4b and Fig.5b show the same simulations where only the value of resistivity is different ($\eta = 10^{-5}$ in the first case and $\eta = 10^{-7}$ in the second). As was illustrated earlier in Fig.2b, at lower resistivity, the growth rate of the ballooning mode decreases significantly, and the first effect which can be seen on filaments is that with a lower growth rate, they do not really cross the separatrix. However, the radial speed of filaments does not vary much between the two cases, only the distance traveled, but at the beginning of the perturbation, the speed is similar (about 2 to 3km/s). So far, no clear mechanism has been identified for the radial speed of filaments.

Nevertheless, it is clear that the ballooning growth rates play a major role concerning the amount of energy evacuated by the filaments, since at lower resistivity, filaments do not even cross the separatrix, so that less energy is ejected from the pedestal. In fact this couples with another particularity of filaments. It has been found that the radial size of filaments, at the beginning of their formation in the pedestal, always corresponds to the width of the pedestal pressure gradient (this was verified with both JET and non-JET simulations). Hence, considering the two cases at high and low resistivity, at the beginning of the crash, the filaments have the same radial width and the same radial speed, but they clearly do not evacuate the same amount of energy in the end. It should also be noted that the fact that filaments do not cross the separatrix is not due to a variation of the amplitude of the poloidal equilibrium flow, which does not change with resistivity [3].

Concerning the poloidal rotation of filaments, a clear quantification of the speed is also hard to

obtain, and it may vary strongly from one case to the other. Also, the relation to the equilibrium poloidal flow is not clear, since the ballooning perturbation itself induces a strong poloidal rotation in the pedestal [1,3]. The poloidal rotation of filaments may vary between 0 up to 3km/s in simulations of JET plasmas, and negative rotation (clockwise poloidally) is often observed. Rotation of filaments during ELMs is clearly observed on tokamaks, using either the fast visible camera on MAST [28], or the ECE-imaging diagnostic on AUG [29], where filaments are observed to rotate with a speed of about 2km/s. It should however be noted that in some simulations of standard plasmas (not JET plasmas), higher poloidal speeds have been observed, up to 15km/s; simulations of JET plasmas have not yet exhibited such high speeds.

3.2 GENERAL RESULTS: DIVERTOR HEAT-FLUXES

The divertor heat-fluxes during simulations of ballooning modes may be compared to what is observed during ELMs with the Infra-Red camera on JET, for Pulse No: 73569 in particular. With the IR camera, during ELMs, narrow heat-flux structures are typically observed near the strike point on the outer divertor. An example of the heat-flux profile along tile 5, during an ELM of Pulse No: 73569, is given in Fig.6a. One particularity of such divertor heat-fluxes is the formation of distinct stripes near the strike point. Such structures are also observed in simulations, as shown in Fig.6b, and it has been shown that, in simulations with strong $\kappa_{||}$, these structures correspond to the perturbation of magnetic field lines [2,30]. In fact, if magnetic field lines are perturbed near the separatrix, $\kappa_{||}$ being higher in the pedestal, temperature becomes almost constant along field lines, so that structures in the magnetic field correspond to structures in the temperature, and thus the heat-flux. In two-fluid simulations, $\kappa_{||}$ is higher for the electron temperature. Hence, where filaments are warm with T_i and cold with T_e, the divertor heat-fluxes, in contrast, are mainly caused by electron temperature. Fig.7 shows the ion and electron temperatures near the X-point during a ballooning mode simulation. The same color scaling is used for the two temperatures, to exhibit the fact that T_i does not reach the divertor as much as T_e. It also should be noted that the number of stripes arriving on the outer divertor depends on the mode number which is simulated. Thus, simulations could be used to help and determine what is the dominant mode number of JET ELMs. Fig.8 shows IR divertor heat-flux profiles from Pulse No: 73569 and from simulations. A scan in mode number with simulations shows that the number of stripes increases with increasing mode number. This increase is linear, with (including the strike point) 4 stripes for n = 8, 6 for n = 12, and 8 for n = 16.

As may be clearly observed on Fig.6a, and as is observed during some ELMs in JET [25], the stripes forming near the strike point are moving on the divertor, towards the lower-field side of the machine. Such movement is also observed during simulations of ballooning modes. The maximum speed of stripes in simulations of JET Pulse No: 73569 was found to be of the order of 200m/s, which is quicker than what is typically observed on JET (about 80-100m/s). However, in simulations such dynamics is reproduced only for a short time, while stripes in JET experiments can move regularly, with almost constant speed, for the whole ELM crash (several hundred microseconds). Such regular

dynamic has yet not been achieved with simulations. Nevertheless, simulations have shown that the dynamics of heat-flux stripes is strongly linked to a poloidal rotation of the ballooning mode. This has been thoroughly verified with simulations of both JET and non-JET plasmas. Fig.9 shows heat-flux stripes moving about 1cm in 50μs, and a mid-plane zoom on a structure in the electric potential, which shows that the ballooning mode is rotating with a speed of about 3km/s at that moment.

In order to give a rough explanation of why rotation of the mode induces heat-flux dynamics, it should be noted that a poloidal rotation of ballooning mode structures may be interpreted as a toroidal rotation: since ballooning modes are aligned with the magnetic field, if a filament structure rotates poloidally, it will intersect the horizontal plane $Z = 0$ at another toroidal angle. Now the heat-flux stripes on the divertor are the footprints of the ballooning mode. As shown on Fig.10a, for the mode number $n = 8$, eight 'fingers' are observed on the divertor, so if the mode rotates toroidally, these fingers will rotate too. Fig.10b shows the same figure stretched out in equal length-scale for the toroidal and radial directions, showing that a toroidal rotation of the 'fingers' will appear like a radial movement of stripes at a given toroidal location. In addition to this interpretation, Fig.11 shows Te stripes on the divertor moving in the other direction, towards the higher-field side, closer to the strike point. This is observed when filaments move in the other direction (clockwise poloidally), which cerftifies that the dynamics of heat-flux stripes is caused by the rotation of the ballooning mode.

3.3 TOWARDS A QUALITATIVE VALIDATION OF SIMULATIONS

It has been shown above (Fig.2b) that the non-ideal MHD parameters may have a significant effect on the linear stability of ballooning modes. In particular, resistivity enhances the activity of MHD modes, so that growth rates become higher at higher resistivity. Therefore, since simulations are usually run at relatively high resistivity, due to numerical stability, simulations of ballooning modes are expected to produce big pedestal crashes. An example of this is shown in Fig.12, which shows a simulation with $\eta = 10^{-6}$, where the ELM-affected area is observed to increase almost without end, so that the ballooning mode penetrates the plasma core much further than what is observed experimentally. For simulations of type-I ELMs, such behaviours should clearly be avoided, which means the resistivity has to be brought down as much as possible. This is numerically difficult for two reasons: firstly, low resistivity means smaller current structures and thus higher requirements on grid resolution; and secondly, since growth rates diminish at lower resistivity, one should make sure that ballooning modes do not become stable at low resistivity.

It turns out that both problems have the same impact: higher requirements on the grid resolution. In the first case, the reason is rather clear, since in order to solve smaller current structures at lower resistivity, one needs more spacial resolution. In the second case, if the ballooning modes are stable at low resistivity, then there are two options. Since it has been checked (Fig.2a) that the JET equilibrium used in simulations is ideally unstable, the reason that it may be stable at low resistivity is that other non-ideal MHD parameters have a stabilizing effect on ballooning modes. As shown in Fig.2b, at higher viscosity μ, the ballooning modes are more stable. This is also true for $D_\perp$ and $\kappa_\perp$. Simulations

are usually run with such parameters set to relatively high values, which is why the modes are stable at low resistivity. To obtain simulations with near-experimental values for $D_\perp$, $\kappa_\perp$ and μ would require very high grid-resolutions, which is not achievable yet. Instead, another possibility consists in increasing the pedestal pressure gradient by diminishing the width of this pressure gradient (within error margins of the HRTS diagnostic), in which case the grid size also has to be increased since higher gradients have to be discretized. This second option is less demanding in terms of grid resolution than trying to lower all diffusive parameters, and it is the one used in the following study. For the case with lowest pressure gradient width (~1.2cm), the radial grid resolution in the pedestal region comes up to 5 elements per cm. The grid resolution in the poloidal direction reaches 0.3 elements per cm.

Mainly two scans have been produced. Since the first goal of the study was to provide some validation of simulations, the scan in collisionality ν^* has been chosen. By measuring the ELM energy losses as a function of collisionality, simulations can be compared to the multi-machine scan produced by Loarte et al. [6], which is at present one of the most robust experimental results about type-I ELMs physics, and which shows that the ELM size increases with decreasing collisionality. The collisionality scan is done in simulations by varying density at constant pressure, so that the ideal MHD stability of the plasma does not change, but the collisionality does. Since temperature is normalized to density ρ_o, this is quite straight forward, and it amounts to a change in the normalization of the whole system of equations. Hence, all non-ideal MHD parameters are varied consistently, and the neoclassical collisionality is changed as $\nu^* \sim \rho_o/T_o^2 \sim \rho_o^3$. In particular, the resistivity and parallel thermal conductivity vary respectively as $\eta \sim \nu^{*1/6}$ and $\kappa_\parallel \sim \nu^{*-1}$. Also, when considering real time from simulations, the correct re-normalized time is used, $t = \tilde{t}\sqrt{\rho_o \mu_o}$.

The first scan was run for the JET equilibrium with collisionality ν^* varying between 0.014 and 0.896, and corresponding resistivity varying between 5.10^{-8} and 10^{-7}. The other parameters were varying respectively as $2.10^{-5} \geq \mu \geq 10^{-5}$, $2.10^{-6} \leq D_\perp \leq 4.10^{-6}$, $2.10^{-6} \geq \kappa_\perp \geq 10^{-6}$ and $4.10^5 \leq \kappa_{\parallel o,e} \leq 6.3 \times 10^3$. Simulations were run at each collisionality for the three mode numbers n = 12, n = 16 and n = 20. The resulting growth rates and ELM sizes (relative to pedestal energy) are plotted in Fig.13, in blue color. [Note that the ELM energy losses, as well as the pedestal energy, are calculated by integration over the whole plasma inside the separatrix]. It can be clearly observed that as ν^* is decreased, the growth rates become smaller, due to the decreasing resistivity. This is sufficient to result in relative ELM sizes that decrease with decreasing ν^*. In other words, simulations show a trend in ELM size opposite to that observed experimentally in [6], which strongly suggests that the effect of resistivity on growth rates should be avoided. As a convention, this first collisionality scan is referred to as the resistive scan.

In order to diminish the effect of resistivity, two modifications were brought to the scan. The first modification is naturally that resistivity was further reduced, with a lowest value of $\eta = 5.10^{-9}$, which corresponds to the lowest collisionality. It is worth noting that after re-normalization, this is equivalent to the physical resistivity $\eta = 2.10^{-8}$, which is a factor 20 from the Spitzer resistivity at 10keV. The

second modification is that the pressure gradient width was diminished from 2.8cm to 1.2cm, so that the pressure gradient was increased by more than a factor two. This agrees with corrections brought by Beurskens et al. to the data processing of the HRTS diagnostic: after reprocessing the data for Pulse No: 73569, the pressure gradient width was found to be 1.3cm, which brings some justification to why the pressure gradient needed to be increased at lower resistivity. (Note that this correction was brought posterior to the simulations [31]). In addition to this modification, the perpendicular mass and thermal diffusivities, $D_\perp$ and $\kappa_\perp$,were adapted to the pressure gradient, so that $D_\perp \sim (\nabla\rho)^{-1}$ and $\kappa_\perp \sim (\nabla T)^{-1}$ in the pedestal region. Thus, the fluxes $D_\perp \nabla\rho$ and $\kappa_\perp \nabla T$ are constant in the pedestal region, so that the pressure gradient remains unchanged at equilibrium (ie. the pressure gradient would not flatten before the ELM crash). The resulting growth rates and corresponding ELM losses are plotted in Fig.13 in red color, for the modes n = 8, n = 12 and n = 16. It is observed that the growth rates are not dominated by resistivity anymore, and that the resulting ELM losses increase with decreasing ν^*, which comes closer to experimental results than the first scan. As a convention, it will now be refered to as the ideal scan - since the ballooning modes are dominated by the pressure gradient, not by resistivity. In fact, since good agreement with experiments is obtained in this case (higher pressure gradient), a good representation of Edge-Localised-Modes should rely on the ballooning rather than peeling theory.

It is important to keep in mind, however, that although this scan gives better agreement with experiments than the first scan, a direct comparison with the scaling by Loarte et al. [6] shows that simulations still need further improvement for proper comparisons with experiments. Mainly, the simulated ELMs are smaller, with relative energy losses reaching up to 5.5% only, while JET type-I ELMs can evacuate more than 20% of the pedestal energy; and the collisionality trend is also weaker, with $\Delta W_{ELM}/W_{ped}$ varying betwee $\nu^{*-0.05}$ and $\nu^{*-0.15}$ in simulations, compared to $\nu^{*-0.45}$ in experiments [6]. Nevertheless, this second scan still comes closer to experiments than the first one, and may well be used to enlarge our understanding of Edge-Localised-Modes. Since the biggest ELM crashes for this scan are those caused by the mode n = 8, the following comparisons between experiments and simulations are done with the n = 8 case.

There are a number of comparisons which can be made between simulation results and experimental observations. Of course, the first comparison of interest is the ELM size, which has been shown to increase with decreasing collisionality. There is another particularity of ELM energy losses that can be compared, and which brings some understanding of the mechanisms that drive energy out of the pedestal: convective versus conductive losses. Typically, it is observed experimentally [6,18] that the increase of convective (density) losses at low ν^* is negligible compared to the increase of conductive (temperature) losses. Simulations show that this is due to the strong increase in k at low ν^*. As observed on Fig.13, the growth rates of mode n = 8 do not exhibit a clear increase or decrease as ν^* is varied, but the ELM size does, because at lower collisionality, $\kappa_\parallel$ is much higher (due to higher temperature), so that more temperature is evacuated from the pedestal. This is illustrated in Fig.14, which shows the density and

electron temperature losses relative to pedestal density and electron temperature respectively.

Another comparison which was done concerns the ELM-affected area. Whereas simulations with high resistivity resulted in high ELM-affected areas, as shown in Fig.12, the ideal scan resulted in ELMaffected areas of 15cm (about 17.5% of the minor radius), which did not change with varying $\nu*$. The fact that ELM-affected area is not affected by collisionality is in agreement with experimental results [18]. In particular, this shows that the ELM energy losses is not linked to the ELM-affected area for type-I ELMs.

Then, one crucial comparison between simulations and experiments concerns the divertor heat-fluxes. Comparison with the Infra-Red camera have shown that despite some qualitative agreements, the boundary conditions at the divertor, as well as the model for parallel and perpendicular transport in the SOL, should be improved for better results. Fig.15 shows the divertor heat-fluxes for the mode n = 8 at three collisionalities. It is observed that the duration of the ELM crash changes with collisionality, and reaches up to 300μs; this is shorter than what is observed with the IR-data for Pulse No: 73569, where ELMs are observed to last between 500μs and several ms (see Fig.6a). Note that this may be due to the fact that only one (non-zero) toroidal harmonic is simulated, which could also explain why relative ELM energy losses in simulations are smaller than in experiments. In the highest collisionality case, a slight decrease of the divertor heat-flux is observed after about 120μs; this is caused by a response of the kinetic equilibrium to the ballooning mode (as studied in [3], the equilibrium poloidal rotation in the pedestal region may have a strong stabilizing effect on ballooning modes). Although this induces a significant decrease in the ballooning activity, it is very brief and is thus not considered as the end of the pedestal collapse. Regarding the amplitude of the heat-fluxes, it corresponds to what is observed in experiments (up to $70MW.m^{-2}$), and the total energy arriving on the outer divertor is 11% of the total energy losses (for the lowest collisionality case), which is also in qualitative agreement with experiments. On the other hand, the wetted area is usually bigger in simulations (about 10cm) than what is observed with the IR-camera (about 5 to 7cm). Also, the wetted area does not change at all with varying collisionality, whereas it has been observed experimentally [32,33] that the wetted area increases with ELM size.

Finally, the last comparison between simulations and experiments is a more general result, about ELM-precursors. For the first time, simulations of ballooning modes have exhibited clear ELM precursors. Typically, simulations are started from an unstable equilibrium, so that the perturbation of toroidal Fourier modes grows exponentially to produce an ELM crash straight away. Here, the perturbation of the ballooning mode grows exponentially until it starts perturbing the equilibrium, at which point the perturbation just stands there for some time, before the real ELM crash appears. This is illustrated in Fig.16a, where the energy of the kinetic equilibrium (n = 0 mode) is plotted as a function of time, together with the kinetic energy of the ballooning mode n = 8. This simulation is that with the lowest resistivity, lowest collisionality (with the biggest ELM losses). It is clearly observed that the precursor lasts as long as the ELM crash itself. During all the precursor, small filaments are formed inside the separatrix, and move poloidally before bursting out. It is yet not

understood what keeps the ballooning perturbation from provoking a crash straight away, but such a result takes simulations still closer to experiments, and shows that simulations of multiple ELM cycles could be obtained with JOREK. In fact, if an equilibrium has a pedestal pressure gradient which is unstable to ballooning modes but does not necessarily produce an ELM crash (at least not directly), then it means that after a first ELM crash, if heating power and density sources force the pressure gradient to increase again, the MHD limit may be overtaken without producing a regular, turbulent relaxation of the plasma. This is exactly what makes it difficult to simulate multiple ELM-cycles: that after the first crash, the system converges towards a constant turbulent relaxation. Such a simulation is shown in Fig.16b, where after the first crash, the heating power and the density source are increased, but the ballooning mode creates a steady turbulent evacuation of energy. After some time, heating power is again increased in the hope of producing a crash, but the system only converges to a higher turbulent relaxation level. The simulation of ELM precursors shows that it may be possible to avoid such behaviours, so that the challenge of multiple ELMs simulations may be solved in future.

OVERVIEW AND CONCLUSION

In the present paper, it was shown how experimental data can be used to produce coherent equilibria for ELMs simulations in JET. The High-Resolution Thomson Scattering diagnostic is particularly useful, since it provides pre-ELM pedestal pressure profiles with good spacial resolution, which is one of the crucial elements for ELMs simulations based on ballooning modes. For this study, the low-collisionality, type-I ELMy H-mode Pulse No: 73569 was simulated, and the resulting JOREK-reconstructed equilibrium was tested for its ideal MHD stability with respect to ballooning modes. It was found that the equilibrium (pre-ELM) pressure gradients are well above the stability threshold. However, it was demonstrated that non-ideal MHD parameters, such as resistivity or viscosity, may have a significant influence on the linear stability of ballooning modes. In addition, the equilibrium poloidal rotation of the pedestal plasma was shown to have a strong stabilizing effect on ballooning modes (ie. growth rates are reduced by the flow). As a consequence, the interplay between the pedestal pressure gradient and the non-ideal diffusive parameters is rather subtle, which means that the best approach consists in simulating plasmas as close to experimental conditions as possible, in order to avoid stable modes as well as artificially large modes.

Some general results were described, first concerning the filamentation of the pedestal plasma into the SOL. It was found that the filaments are warmer with ion energy than electron energy (in simulations) due to the higher parallel conduction of electrons - $\kappa_{\parallel,e}/k_{\parallel,i} \sim 40$. A large amount of current is usually evacuated from the plasma, and the maximum of current is localized at the front of the filament. The current density in these filaments may reach large fractions of the pedestal current (up to 80% of the pedestal current in some cases). As an example a case was presented, where the pressure filaments does not cross the separatrix, but the current component of the filament clearly reaches the SOL. Also, one of the characteristics of filaments is that they may rotate poloidally

with high speeds (several km/s). In particular, it was shown that this rotation induces a motion of the heat-fluxes on the outer divertor. Because the ballooning mode perturbs the separatrix, the high parallel conductivity for T_e results in the formation of stripes near the strike point: as the mode rotates, these structures move on the divertor. The speed of these motions was compared to measures of the Infra-Red camera on JET.

In order to obtain some qualitative validation of simulations, the JET equilibrium Pulse No: 73569 was used as a basis for collisionality scans. The scans were produced by varying density and temperature at constant pressure, and resulted in the identification of two distinct regimes. The first resistive regime is found to be dominated by resistivity, so that as collisionality is lowered, temperature increases and so resistivity decreases. Since resistivity 'excites' MHD modes, at lower collisionality, the ballooning growth rates are smaller, and the resulting ELM energy losses decrease, which is the opposite of what is observed experimentally for type-I ELMs [6]. In a more ideal regime, were resistivity is decreased to near-experimental values, and the pressure gradient is taken to be the steepest of what is observed with the HRTS (for Pulse No: 73569), the growth rates of ballooning modes are not dominated by resistivity anymore, and the ELM size (relative to pedestal energy) is observed to increase with decreasing collisionality. In fact, at lower collisionality, the parallel thermal conductivity significantly increases, so that more temperature is evacuated. This is in good agreement with general experimental results [6,18], which state that at lower ν^*, ELMs become conductive rather than convective. In addition, for this ideal scan, it was observed that the ELM-affected area is not affected by collisionality, which is also in agreement with experiments. However, although some reasonable agreement was obtained for the divertor heat-fluxes (time scales and amplitude of fluxes agree with the IR-camera), it was found that the wetted area does not increase with the ELM size, which is not the case experimentally. Such differences hint that the fluid transport model used in JOREK should be improved, possibly to include some kinetic effects, since the Braginskii model [23] is not sufficient to reproduce the divertor heat-fluxes with satisfying accuracy.

One particular result obtained at low resistivity, low collisionality, shows that multiple ELM-cycles simulations could be obtained in near future with JOREK: ELM precursors are observed before the ELM crash. Since simulations are started from an ideally unstable equilibrium, with very steep edge pressure gradients, it is generally expected that the perturbation of toroidal Fourier modes will result in exponential growth of a ballooning mode, leading to a pedestal crash. In some simulations, it was observed that the perturbation does grow exponentially, but that once it starts perturbing the kinetic equilibrium (so that filaments start forming inside the separatrix), the perturbation remains mild, and does not produce a pedestal crash straight away. The ELM precursor lasts as long as the ELM crash itself. Such precursors mean that it is possible to produce simulations were the pedestal pressure gradient progressively increases (as in experiments), and slowly overtakes the ideal MHD threshold without producing some steady turbulent relaxation, so that once the pressure gradient is well above the stability threshold, one obtains a large ELM crash. Simulations of such scenarios will be attempted in the near future.

ACKNOWLEDGEMENT

This work, as part of the project ANR-CIS.2006.001, has benefited from financial support from the French 'Agence Nationale de la Recherche'. It is supported by the European Communities under the contract of Association between EURATOM and CEA, and was carried out within the framework of the European Fusion Development Agreement. The views and opinions expressed herein do not necessarily reflect those of the European Commission.

REFERENCES

[1]. G.T.A. Huysmans and O. Czarny, Nuclear Fusion **47** 659-666 (2007)
[2]. G.T.A. Huysmans et al., Plasma Physics and Controlled Fusion **51** 124012 (2009)
[3]. S.J.P. Pamela et al., Plasma Physics and Controlled Fusion **52** 075006 (2010)
[4]. B. Bazylev et al., Physics Scripta T128 229-233 (2007)
[5]. ITER Physics Basis Editors and ITER EDA, Nuclear Fusion **39** 2175 (1999)
[6]. A. Loarte et al., Plasma Physics and Controlled Fusion **45** 1549-1569 (2003)
[7]. S. Saarelma et al., Plasma Physics and Controlled Fusion **51** 035001 (2009)
[8]. P. Snyder et al., Nuclear Fusion **49** 085035 (2009)
[9]. G.T.A. Huysmans et al., Physics of Plasmas **8** #10 p4292 (2001)
[10]. H.R. Wilson et al., Physics of Plasmas **9** #4 p1277 (2002)
[11]. A. Webster et al., Physical Review Letters **102** 035003 (2009)
[12]. G.T.A. Huysmans et al., Plasma Physics and Controlled Fusion **47** 2107-2121 (2005)
[13]. H.R. Wilson et al., Physical Review Letters. 92 #**17** 175006 (2004)
[14]. O. Garcia et al., Phys. Plasmas **13** 082309 (2006)
[15]. A.Y. Pankin et al., Plasma Physics and Controlled Fusion **49** S63-S75 (2007)
[16]. P. Beyer et al., Physical Review Letters **94** 105001 (2005)
[17]. B. Dudson et al., Plasma Physics and Controlled Fusion **50** 124012 (2008)
[18]. M.N.A. Beurskens et al., Nucl. Fusion **49** 125006 (2009)
[19]. G.T.A. Huysmans et al., Proc. CP90 Conf. on Comp. Phys. Proc. p371 (1991)
[20]. O. Czarny and G.T.A. Huysmans, Journal of Computational Physics **227** 74237445 (2008)
[21]. P. Henon et al., Parallel Comp. **34** 345362 (2008)
[22]. H.R. Strauss, Physics of Fluids **19** 134 (1976)
[23]. J. Wesson, Tokamaks, 3rd ed., Oxford Univ. Press (2004)
[24]. H.R. Strauss, Journal of Plasma Physics, Vol. **57**, part 1, pp 83-87 (1997)
[25]. S. Devaux et al., 36th EPS Conf. on Plasma Phys., Sofia, ECA Vol. 33E, p-2.157 (2009)
[26]. T. Eich et al., Physical Review Letters **91** 195003 (2003)
[27]. O. Sauter et al., Physics of Plasmas **6** 2834 (1999)
[28]. A. Kirk et al., Plasma Physics and Controlled Fusion **49** 1259-1275 (2007)
[29]. J. Boom et al., 37th EPS Conf. on Plasma Phys., Dublin, (2010)
[30]. G.T.A. Huysmans et al., 36th EPS Conf. on Plasma Phys., Sofia, (2009)

[31]. M.N.A. Beurskens et al., 52th APS Division of Plasma Phys. Conf., Chicago, USA, (2010)
[32]. T. Eich et al., 19th Int. Conf. on Plasma Surface Interactions, San Diego, USA, (2010)
[33]. H. Thomsen et al., 23rd IAEA Fusion Energy Conf., Daejon, Rep. of Korea, (2010)

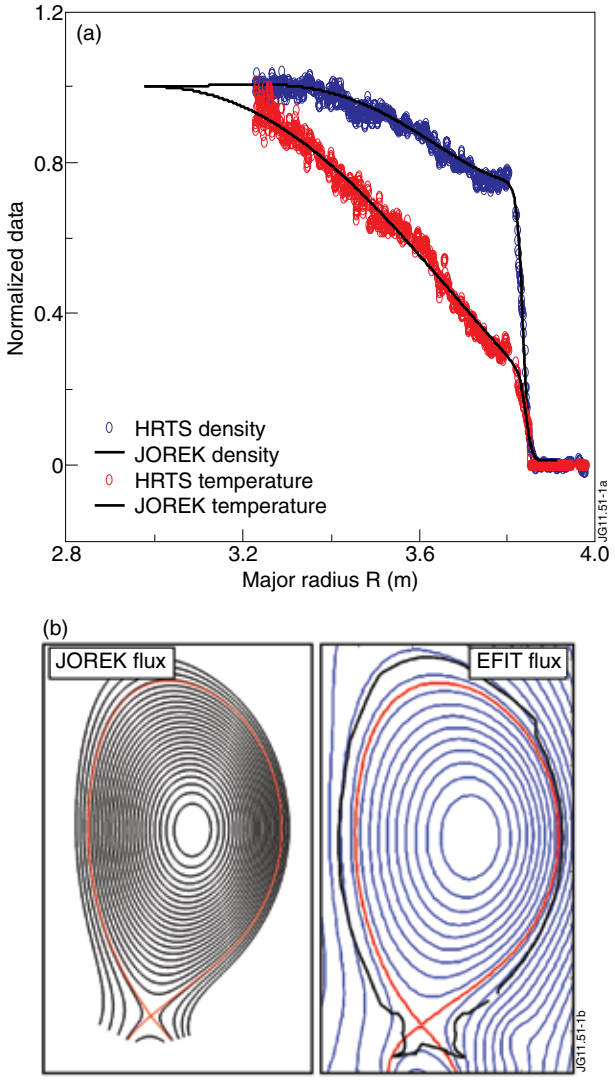

Figure 1: a). The density and temperature profiles from the HRTS diagnostic for the JET Pulse No: 73569 (blue and red circles respectively), with the corresponding fitted profiles used for simulations (plain black lines). b). Flux surfaces of the Grad-Shafranov equilibrium resulting from the reconstruction with JOREK, and the comparison with the EFIT equilibrium reconstruction.

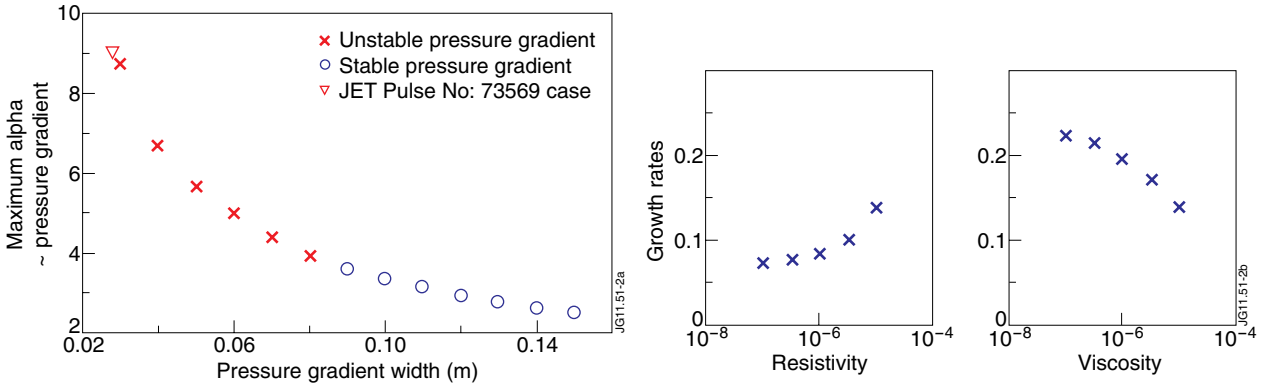

Figure 2: a). A scan in the pedestal pressure gradient width shows that the JET equilibrium Pulse No: 73569 reproduced in simulations stands well above the ideal MHD stability limit (as calculated with the equilibrium code HELENA). b). The growth rates of the ballooning mode n = 12 as a function of resistivity and viscosity. These two scans reveal the important role played by non-ideal MHD parameters with respect to linear stability of ballooning modes.

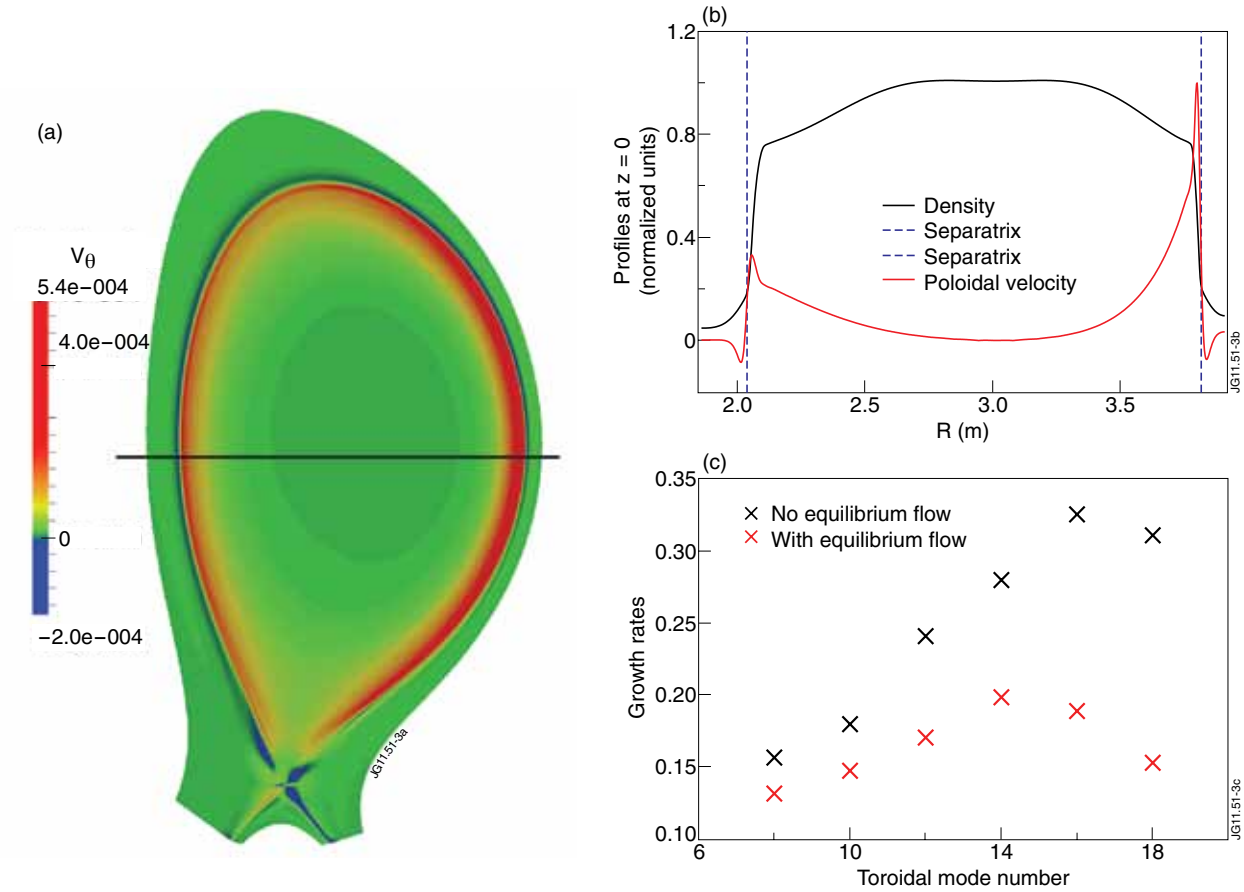

Figure 3: a). The structure of the equilibrium polodal rotation in simulations of JET is typically m = 0. This flow is strongly sheared, with a positive component inside the separatrix and a negative component outside. Units are normalized as explained in Section1.2, so that the maximum velocity corresponds to about 250m/s. b). The corresponding mid-plane profile for the poloidal velocity and the density are plotted to illustrate that the flow is strongly sheared and localised at the pedestal pressure gradient. c). The effect of the equilibrium poloidal rotation on the linear stability of ballooning modes is calculated by running simulations with and without equilibrium flow. The damping effect of the flow on growth rates is strongest for high ballooning mode numbers.

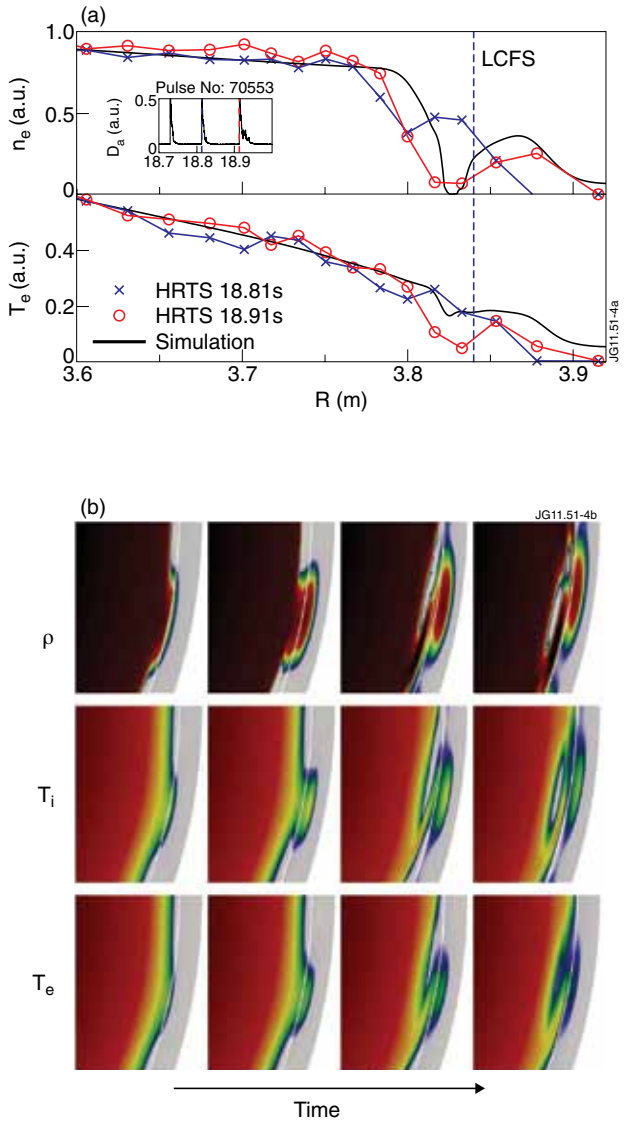

Figure 4: a). Mid-plane profiles of density and electron temperature are taken for a filament in a simulation of JET. The comparison with HRTS profiles shows that the size and composition of filaments is reasonably reproduced by simulations. In particular, the gap of density behind the filament is reproduced, which shows that the filament clearly separates from the main plasma. Since no such filament was observed with HRTS for the Pulse No: 73569, comparisons are made with Pulse No: 70553. Units are arbitrary. b). The time evolution of a filament is plotted for density, ion and electron temperatures, to illustrate the effect of high parallel thermal conductivity on T_e. The electron temperature is evacuated from the filament more rapidly than the ion temperature.

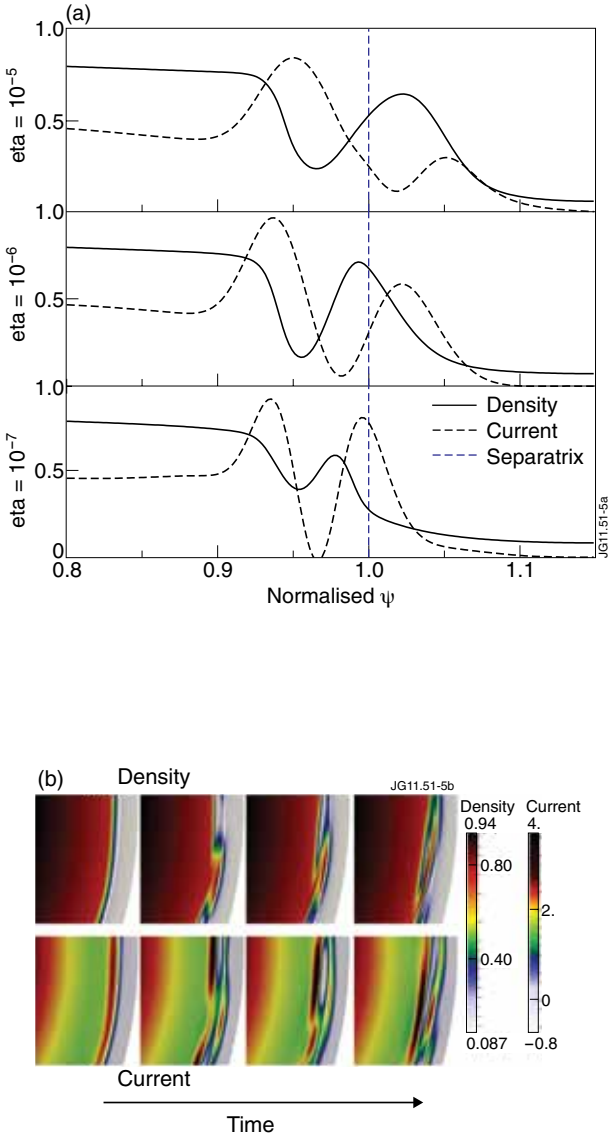

Figure 5: a). HRTS-like mid-plane profiles of filaments for different values of resistivity. The density and current are plotted together to show that the current is localised in front of the density filament. Such behaviour was not observed in previous simulations of standard plasmas, even JET-like plasmas. In previous simulations, the density and current were in phase. b). At lower resistivity ($\eta = 10^{-7}$), the growth rates are smaller, so that the density filament does not really cross the separatrix, and is instead sheared off by a poloidal flow. In such cases, almost no pressure crosses the separatrix, but a current filament is clearly ejected across the separatrix. This illustrates not only that the current is localised in front of the density, but it also shows that with low growth rates, filaments do not reach so far across the separatrix.

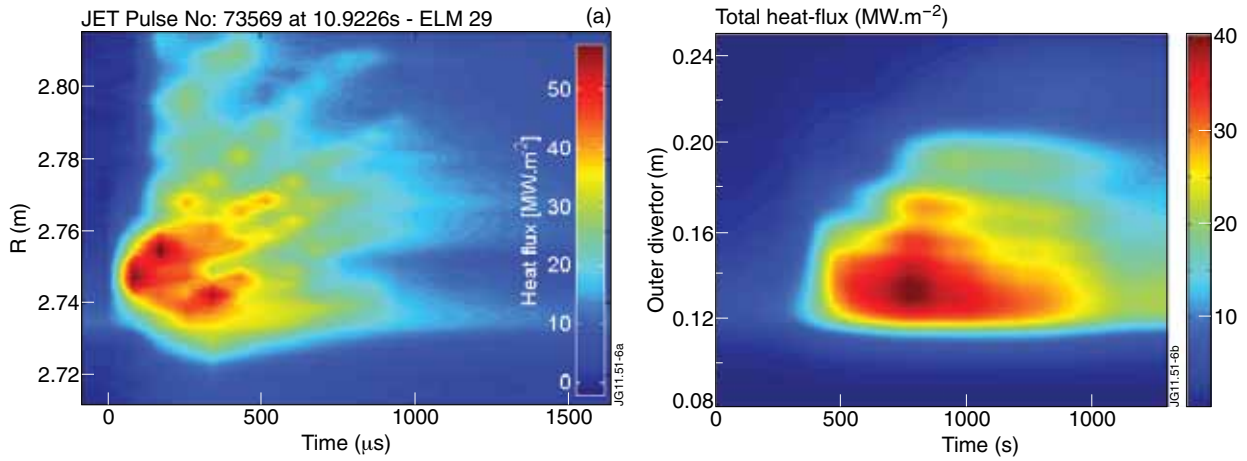

Figure 6: a). Infra-Red Camera profile of the divertor heat-flux, plotted as a function of time, for an ELM of JET Pulse No: 73569. Stripes are formed near the strike point, and move towards the lower-field side during the ELM. Such heat-flux dynamics is sometimes observed on JET [25]. b). Simulations of JET Pulse No: 73569 also exhibit such heat-flux stripes near the strike point on the outer divertor.

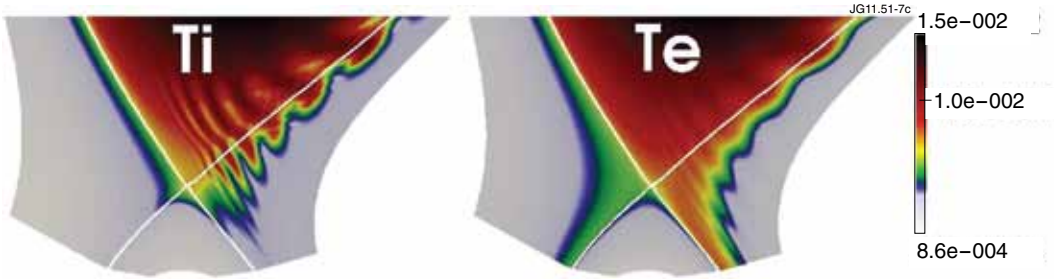

Figure 7: Comparison of ion and electron temperatures near the divertor during a simulation of a ballooning mode for JET Pulse No: 73569. T_e is rapidly conducted along field lines to the divertor, more than T_i, due to higher $\kappa_{\|}$ for electron temperature. The same color scaling has been used for both temperatures.

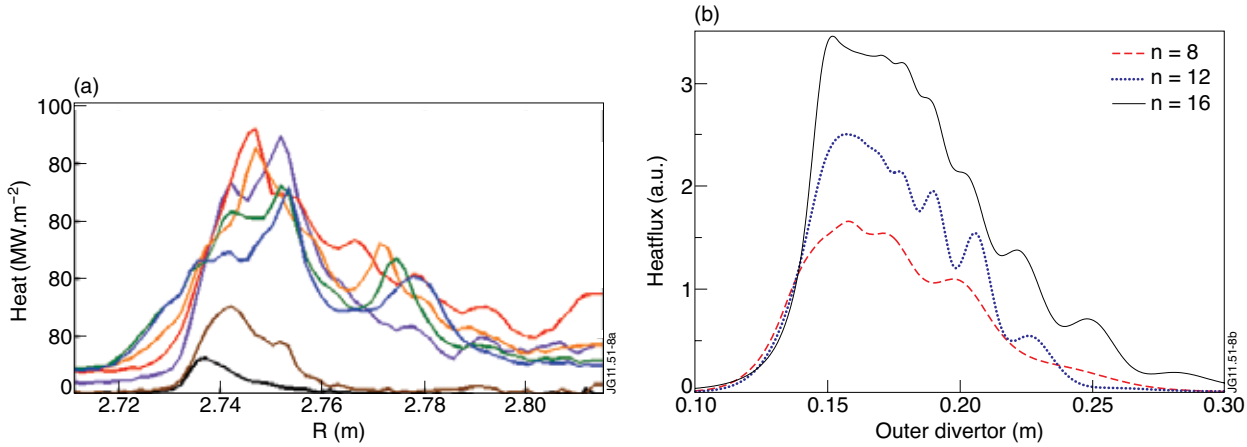

Figure 8: a). Heat-flux profiles measured by the IR-camera during an ELM of JET Pulse No: 73569, showing stripes near the strike point. b). The number of heat-flux stripes in simulatons varies with the ballooning mode number. Simulations could be used to help and determine the dominant mode numbers in JET ELMs.

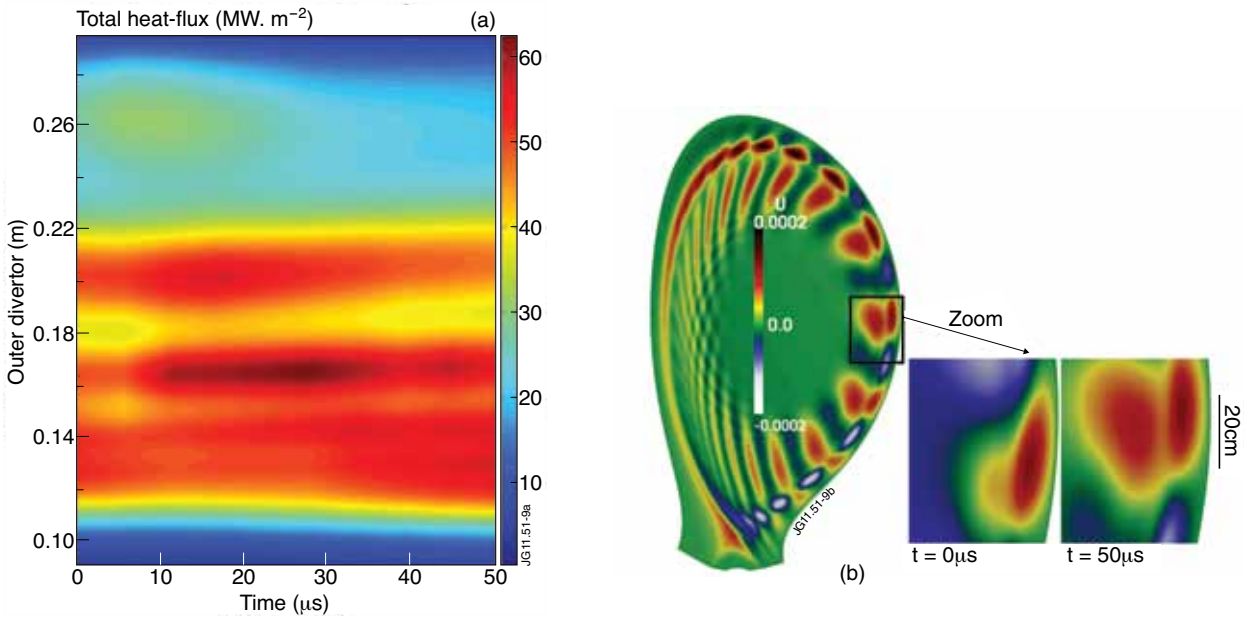

Figure 9: a). Heat-flux stripes moving on the outer divertor with a speed of ~200m/s. b). The rotation of the ballooning mode in the poloidal plane during this time is about 3km/s. Shown here is the electric potential Φ (defined as u in simulations), with a zoom on a filament structure.

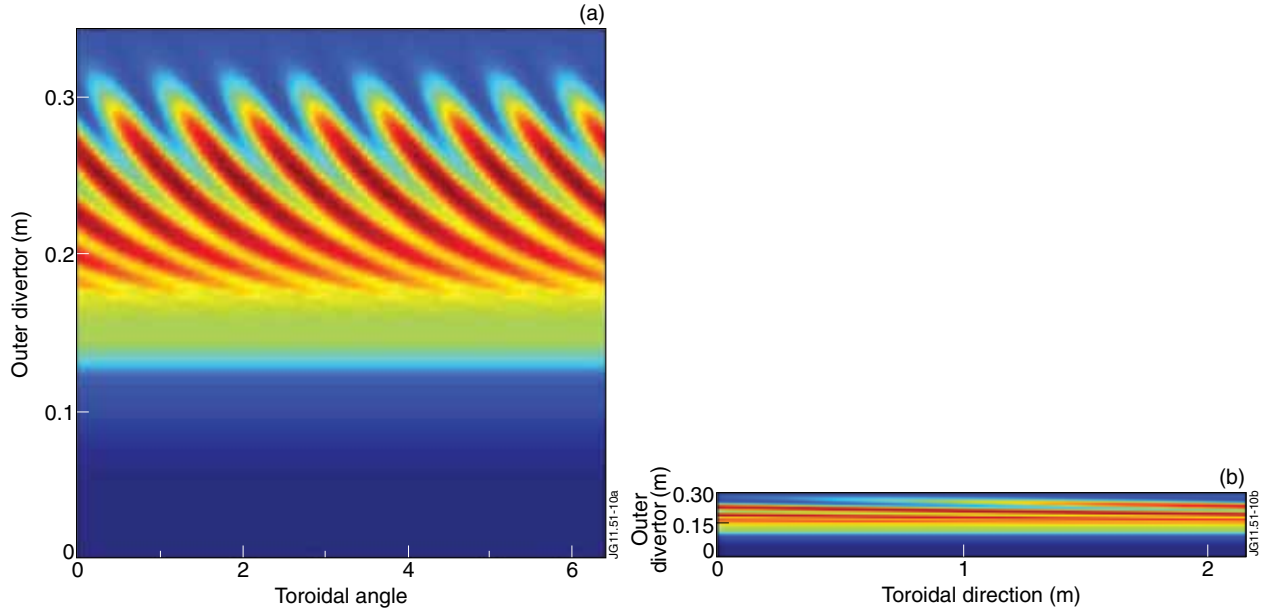

Figure 10: a). The same number of T_e 'fingers' are observed on the divertor as the mode number. This simulation is that of the mode n = 8. As the ballooning mode rotates poloidally/toroidally, these 'fingers' move on the divertor. b). Stretched out to equal length-scale for the toroidal and radial directions, the same plot reveals how toroidal rotation of stripes may be interpreted as a radial displacement when looking at one specific toroidal location on the divertor.

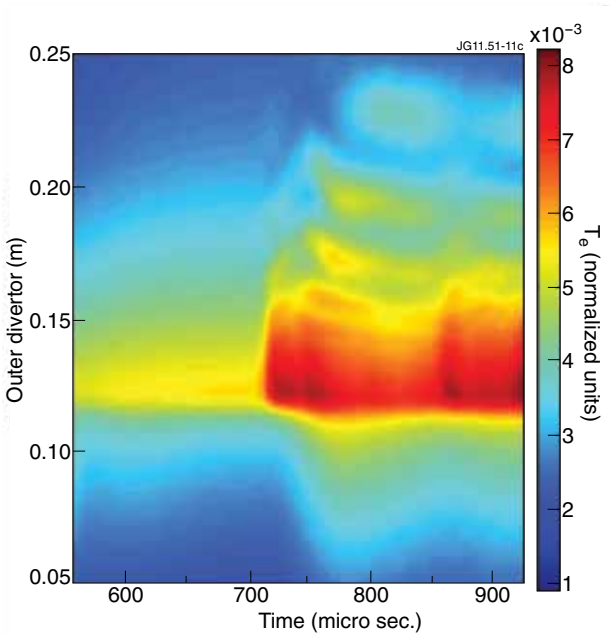

Figure 11: As a demonstration that the dynamics of heat-flux stripes is caused by the rotation of the ballooning mode, this figure shows T_e stripes moving in the opposite direction on the divertor (closer to the strike point): this is observed simultaneously with a rotation of the ballooning mode in the opposite direction (clockwise poloidally).

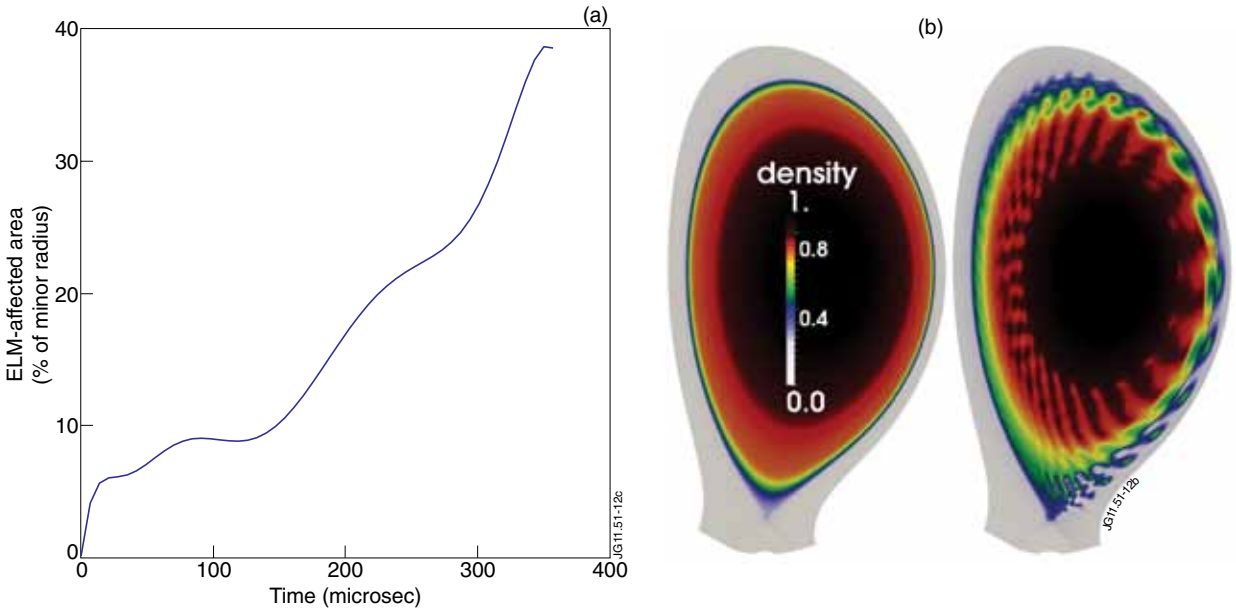

Figure 12: a). ELM-affected area as a function of time, during a simulation with relatively high resistivity ($\eta = 10^{-6}$). b). The corresponding density at time t = 0 (left) and at time t = 350μs (right), to exhibit how far into the core the ballooning perturbation may reach.

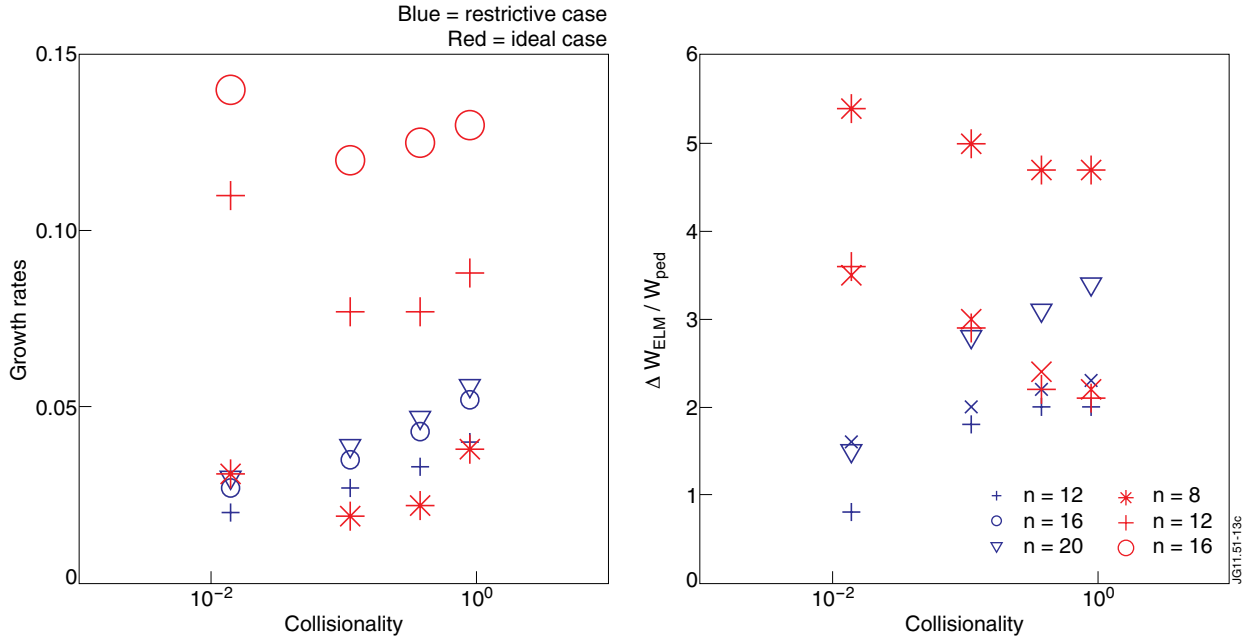

Figure 13: This figure shows a plot of the ballooning growth rates as a function of ν (left), together with the corresponding ELM sizes, relative to pedestal energy (right). The thin blue symbols correspond to the scan with high resistivity, while the thick red symbols correspond to the scan with lower resistivity. The scans were run for different mode numbers, ranging from n = 8 to n = 20.*

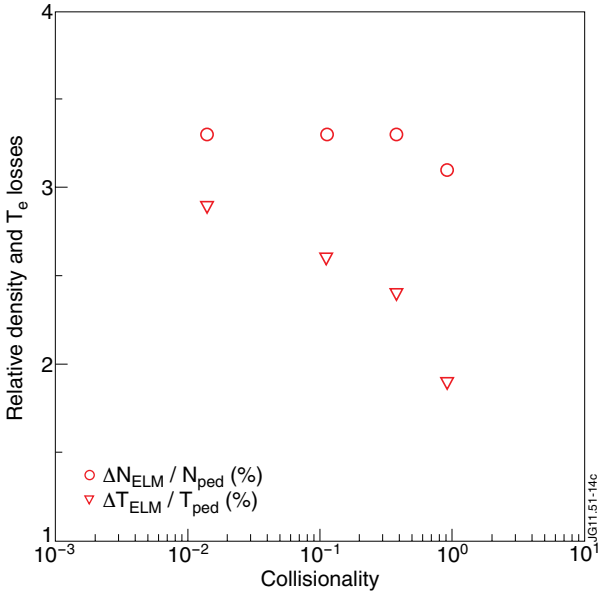

Figure 14: The relative density and electron temperature losses as a function of collisionality for the mode n = 8. Density losses remain constant while electron temperature losses clearly increase, due to higher $\kappa_{||}$ at lower collisionality.

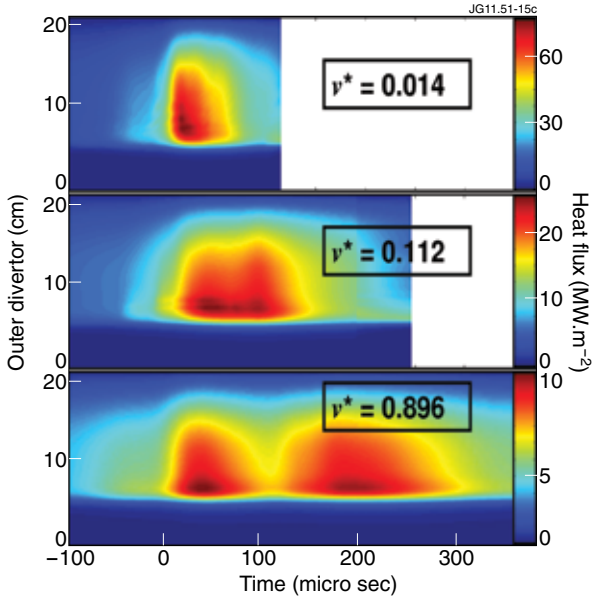

Figure 15: The outer divertor heat-flux for the mode n = 8 at three different collisionalities. Time has been translated to start at the ELM onset.

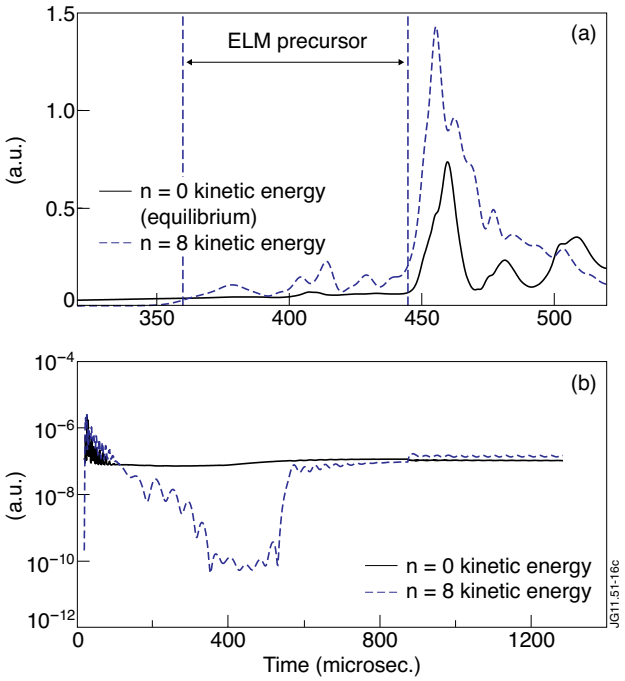

Figure 16: a). An ELM-precursor is observed, as the kinetic energy of both the equilibrium n = 0 and the ballooning mode n = 8 are plotted as a function of time. The precursor is observed to last as long as the ELM crash itself. b). Some attempts of simulating multiple ELM cylcles have often resulted in a convergence towards a steady, turbulent relaxation of the pressure gradient. In this example, after some time, heating is further increase, in the hope of producing a real pedestal crash, but the system converges to another level of steady turbulence. The simulation of ELM precursors means that such behaviour could be avoided, since a plasma can stand at the stability limit without producing a crash.